EasyChair Preprint

№ 3573

A Weighted Variance Approach for Uncertainty Quantification in High Quality Steel Rolling

Peng Wang, Yueda Lin, Ree Muroiwa, Simon Pike and Lyudmila Mihaylova

June 7, 2020

A Weighted Variance Approach for Uncertainty Quantification in High Quality Steel Rolling

Peng Wang*, Yueda Lin*, Ree Muroiwa†, Simon Pike†, and Lyudmila Mihaylova*

*The University of Sheffield, Sheffield, UK. Email: {peng.wang, ylin42, l.s.mihaylova}@sheffield.ac.uk
† Liberty Speciality Steel. E-mail: {ree.muroiwa, simon.pike}@specialityuk.com

***Abstract*—This paper proposes a computer vision framework aimed to segment hot steel sections and contribute to rolling precision. The steel section dimensions are calculated for the purposes of automating a high temperature rolling process. A structured forest algorithm along with the developed steel bar edge detection and regression algorithms extract the edges of the high temperature bars in optical videos captured by a GoPro® camera. To quantify the impact of noises that affect the segmentation process and the final diameter measurements, a weighted variance is calculated, providing a level of trust in the measurements. The results show an accuracy which is in line with the rolling standards, i.e. with a root mean square error less than $2.5\ mm$.**

***Index Terms*—Manufacturing and automation, Metrology, Computer vision, High temperature steel production, Uncertainty quantification**

I. Introduction

An Automated, Intelligent, Online-decision-making, and Non-contact (AI-ON) measuring system is critical to automating steel rolling processes, and to operational-cost reduction. Such systems have higher efficiency compared with traditional rolling systems with contact-based measuring methods and protect human operators from hazardous environments.

Among non-contact measuring methods, Light Detection And Ranging (LiDAR) based methods such as [1], have demonstrated high accuracy. However, this comes with a significant economical cost. Alternatively, computer vision methods provide high accuracy and are inexpensive. For instance, by projecting structured light onto steel bar surfaces, the method developed in [2] is able to measure the diameter of a 53 tonnes round steel bar with a maximum error of 0.38%. Liu et al. [3] propose an approach for online diameter estimation of cylindrical forgings, obtaining relative errors less than 0.7%. Similarly, Yang et al. [4] propose a method that shows improved measurement accuracy of rectangular forgings, attaining an average 0.48% estimation error. Since the encoded structured light can be easily perceived as intense light, this approach cannot be used easily in rolling applications where there are various intense light sources.

To avoid the disadvantages of the aforementioned measuring systems, Zatočilová et al. [5] design a passive, stationary multi-image system for fast measuring of dimensions and straightness of rotationally-symmetric forgings. An edge detection algorithm that exploits simple shapes of the forging is developed. After extracting four boundary curves of the forging in a pair of images, a 3D model reconstruction is performed where the length, diameter, and straightness of the forgings are calculated. The system is proved capable of performing diameter measuring with deviations less than 1%. Wu et al. [6] propose a monocular-vision-based method for online measuring of a weld stud. An accurate mathematical model constrained by the measuring principle is developed. Based on the model, a further calibration is proposed to optimise the projective transformation parameters. They show that the model is flexible, fast, and capable of achieving high-precision measurements of the weld stud. Nevertheless, the temperature in these two cases is not as high as to 1000 - 1500°C, at which the intense radiation of the Hot Rolled Bar (HRB) can cause overexposure problems easily. Figure 1 shows video frames

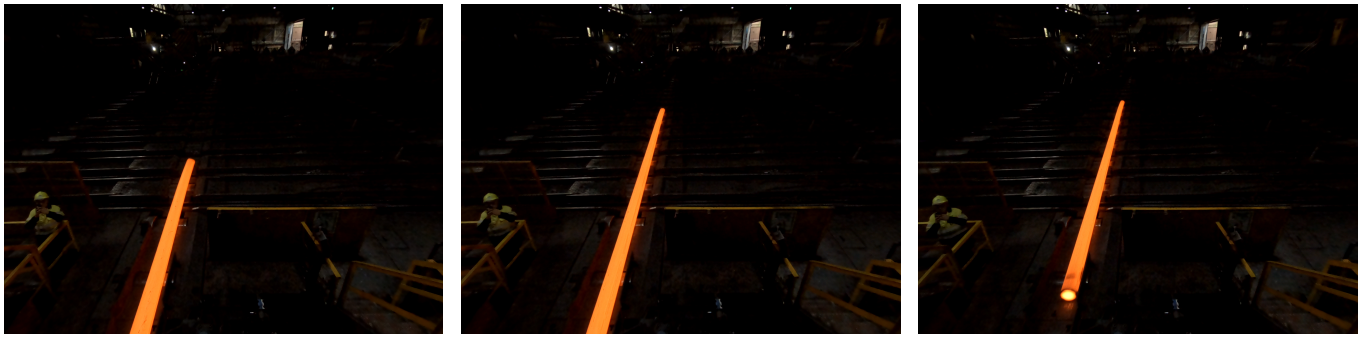

(a) (b) (c)

Fig. 1. Hot rolled bars whose size is estimated remotely

of such HRBs. Due to the high temperature radiation and the HRBs are cooling down unevenly while moving on the conveyor, the edges of the HRBs are often blurred.

This paper presents a framework for high temperature HRB size measuring with a non-industrial GoPro® camera, and gives a level of trust in the obtained results. The framework can be applied in low-cost non-industrial devices for automating the high quality steel rolling process. We start by presenting the algorithm for extraction of the boundaries of interest to detect and extract the edge boundaries of HRBs. The boundaries of interest define an 'area' where the HRB edges are most likely to be, which makes the algorithm more resilient to environmental changes, such as to glare and changes of the lighting conditions. The proposed sliding window random regression algorithm applies random regression within the Current Boundary Of Interest (CBOI), which is defined as the region enclosed by the current sliding window and boundaries of interest, to fit the HRB edges.

The challenges faced include: *1*) Multiple edges are detected as shown in Figure 2; *2*) Edges detected are diffuse [7]. Both challenges lead to accuracy degradation. This makes a regression model necessary to fuse pixel-wise information and fit line segments to them. Pixel coordinates of the fitted line segments are then transformed into the physical plane for dimension calculation, with the help of translation and rotation matrices obtained from camera calibration. However, while boundaries of interest constrain the possible locations of the edges, they also bring in uncertainties to measurements. We have applied the sliding window random regression algorithm to concentrate pixel-wise information to reduce the impact of uncertainties. The uncertainty is then quantified by the weighted variance algorithm to provide a level of trust in the achieved results.

The main contributions of this work are: ***1***) A framework for automating the sizing process of steel bars in a high-temperature rolling process is proposed; ***2***) A weighted variance algorithm is developed to quantify the impact of uncertainties on the measurements; ***3***) The proposed framework is evaluated and validated over real data from a rolling process for high quality steels.

The remaining part of the paper is structured as follows. Section II describes how the HRBs are detected, and the sliding window random regression algorithm that determines the edges is presented. The algorithm for uncertainty quantification is given in Section III. Section IV presents the algorithms performance validation and evaluation, and Section V concludes the paper.

II. Edge Detection and Random Regression

A. Edge Detection

In spite of the existence of both traditional edge detection methods [8] and the current deep learning based state-of-the-art edge detection methods [9], we adopt the structural random forests algorithm [7] to extract edges in the video frames. Compared with traditional edge detection methods whose performance relies on setting up good thresholds, the structural random forests algorithm can provide relatively stable and adaptive results without setting up parameters. In addition, the structural forests can deal with Red, Green, Blue (RGB) images directly, while traditional edge detection methods such as Canny require to convert RGB images to gray scale images, which would limit the efficiency. Compared with deep learning based edge detection methods, the structural random forests algorithm is easier to train, lighter to be deployed, and less dependent on expensive hardware like GPUs.

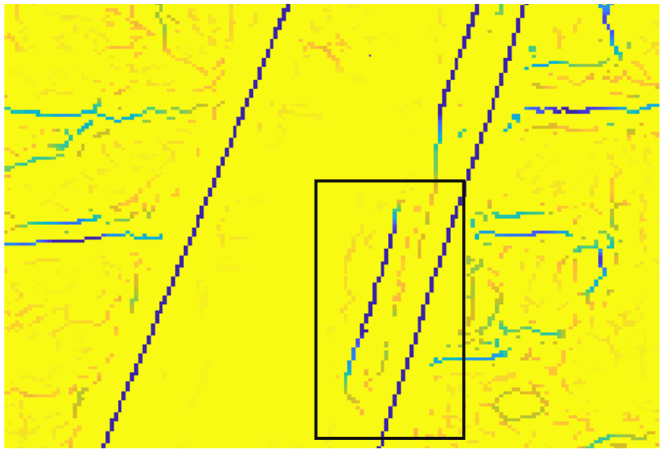

Fig. 2. Edges detected by the structural random forests. The black rectangle shows that more than one edges are detected, where only one is expected. Prominent edges are marked in dark blue, while other weak edges are marked in light colours.

Edges detected by the structural random forests provide inputs to our proposed measuring framework. Both HRB edges and environment edges are detected at this stage. Preliminary results with the structural random forests algorithm [7] and with thermal images are reported in our preceding paper [10]. The main idea is to detect edges in images via constructing a structured forest. One of the disadvantages of the structured forest algorithm, as discussed in [7], is the occurrence of diffused edges, which causes accuracy degradation. We implement the algorithm by enabling the Non-Maximum Suppression (NMS) [7] to sharpen the extracted edges. Figure 2 shows sharpened edges from the structural random forests algorithm. Three types of edges are detected: *1*) Edges of the HRB, which are the two longest edges marked in dark blue. *2*) Strong non-HRB edges, e.g., the dark blue edge apart from the HRB edge within the rectangle. *3*) Weak non-HRB edges, e.g., all edges apart from the two strong ones.

The hot steel bars, however, have only two prominent edges and we need well pronounced edges in order to calculate the diameter of a cylindrical bar. As it can be seen within the rectangle shown in Figure 2, there are more than one detected edges, although we are expecting just one. The reasons for this ambiguity are twofold. From the HRB aspect, while rolling along the conveyor, the HRB is cooling down unevenly. This results in intensity changes in the images and hence leads to extra 'edge' detection by the algorithm. From the structural random forests algorithm aspect, Dollar et al. [7] explain that

the edges can be diffused due to the fact that edge estimation can shift a few pixels from the true location. The underlying cause is that the voting mechanism used cannot ensure the noisy edge predictions to be well aligned. This also causes weak edges (marked in light colours) as shown in Figure 2.

To mitigate the effects of those extra edges and to achieve high accuracy in the measurements, a sliding window random regression algorithm is further applied to process the edges detected by the structural random forests.

B. Sliding Window Random Regression

To find the edges of interest, which are edges of a HRB, in a given frame I_{RGB}, we propose Algorithm 1 to subtract the background and get boundaries of interest of the HRB edges. In order to do that, I_{RGB} is binarised according to [11] based on histogram information, resulting in I_{BW}. It is then processed with opening morphological methods followed by a dilation [12] to remove imperfections, caused by temperature diffusion and background noises. The resulted I_{MOR} is applied to mask the edges I_{EDGE} detected by the structural random forests, resulting in I_{GEDGE} with mainly edges of the HRB.

To remove weak edges, pixels in I_{GEDGE} with intensities less than a threshold β are suppressed. Edges in I_{GEDGE} are further binarised and denoised with morphological methods resulting in I_{MEDGE}. Figures 3 (a) and (b) show examples of edges detected by Algorithm 1. We can see that edges of HRBs become prominent and most weak edges are removed. However, there are still environmental edges that mix up with the HRB edges. They are caused by the cooling process. Their intensities are usually weaker than those of the HRB edges, while still stronger than those weak edges. If we set up the parameters of Algorithm 1 to be with high values, there is a risk that the HRB edges are removed as well. We, therefore, set up moderate values of the parameters in Algorithm 1 to remove weak edges.

Next, we use the Moore-Neighbor tracing algorithm [13] to extract the boundaries of interest I_{BOI} of I_{MEDGE} and to make sure that HRB edges are enclosed within the boundaries of interest. Figures 3 (c) and (d) show in green the extracted boundaries of interest. Obviously, the presence of environmental 'edges' is inevitable. This, however, makes the remote sizing even more challenging and increases the necessity of uncertainty quantification of the measurements.

With boundaries of interest obtained from Algorithm 1, we now give details of the sliding window random regression algorithm in Algorithm 2. We define a binary sliding window $I_{H\times W}$ (shown in white in Figures 3 (c) and (d)) with height H and width W to select a region of interest for the sliding window random regression algorithm. Considering the background is subtracted by Algorithm 1 and the HRB moves vertically, W can be set to the width of the image. In this paper, we set up the sliding stride to be equal to H without loss of generality, and assume that the sliding window $I_{H\times W}$ can move m steps in total.

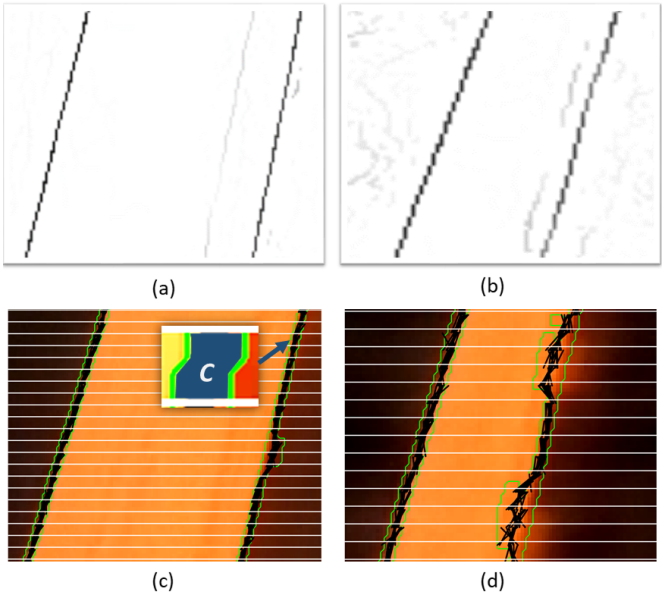

Fig. 3. Results of the sliding window random regression algorithm. (a) and (b) are the edges detected by Algorithm 1. (c) and (d) show the sliding window random regression results, where the green curves are boundaries of interest, white lines indicate the sliding windows, and black line segments are from sliding window random regression algorithm. (c) also shows a CBOI with its area marked in dark blue, and the area is denoted by C.

Algorithm 1 Boundaries Of Interest Extraction

Input: I_{RGB}

Output: Detected HRB edge boundaries I_{BOI}

1: Binarise I_{RGB} according to Otsu's method $\rightarrow I_{BW}$ [11]
2: Morphological denoising $I_{BW} \rightarrow I_{MOR}$
3: Structural Random Forests with NMS enabled $\rightarrow I_{EDGE}$
4: Mask I_{EDGE} with I_{MOR} and convert the result to grey-scale $I_{GEDGE} = I_{MOR} \odot I_{EDGE}$
5: Strength edges in I_{GEDGE}
6: Morphological denoising $I_{CEDGE} \rightarrow I_{MEDGE}$
7: Moore-Neighbor Tracing Algorithm to extract boundaries of $I_{MEDGE} \rightarrow I_{BOI}$.

For the i-th sliding window $I_{H\times W}$, with $i \in \{1, \cdots, m\}$, we suppose that there are n_i HRB edges within it. For the j-th HRB edge, with $j \in \{1, \cdots, n_i\}$, there is a corresponding CBOI that encloses the HRB edge. Figure 3 (c) shows an example of CBOI in the center of the figure. It is enclosed by the current sliding window edges (on the top and bottom of the dark blue area) and boundaries of interest (on the left and right of the dark blue area). We denote the left and right edges of the CBOI as B_j. The coordinates belong to B_j are then concatenated as $\hat{\mathbf{x}}_{ij}$ and $\hat{\mathbf{y}}_{ij}$, which are further classified by the K-means algorithm [14] into several clusters, depending on the number of HRB edges.

As it can be seen from Figures 3 (c) and (d), the HRBs are not segmented well due to the unevenly cooling process and other factors. This directly leads to corrupted CBOIs, or expansion of CBOIs. It would ultimately degrade the accuracy

Algorithm 2 Sliding window Random Regression of Hot Rolled Bar Edges

Input: I_{BOI}, a binary sliding window $I_{H\times W}$
Output: $\mathbf{x}_{ij}$, $\mathbf{y}_{ij}$, $i = 1, \cdots, m$, and $j = 1, \cdots, n_i$.

```
for i = 1, ..., m do
    Determine the HRB edges number n_i within I_{H×W}
    for j = 1, ..., n_i do
        Concatenate the coordinates of B_j as x̂_ij and ŷ_ij.
        Using k-means to classify x̂_ij and ŷ_ij into two
        clusters, each corresponds to a HRB edge.
        Linear regression
            f_ij(x) = a_ij x + b_ij
        Re-calculate y coordinates from row (i−1)∗H+1
        to row i∗H within the sliding window
            x_ij = [(i−1)∗H+1, ..., i∗H]
            y_ij = a_ij x_ij + b_ij
    end for
end for
```

of the calculated diameters of the steel sections. Thus, we randomly sample S point pairs from $\hat{\mathbf{x}}_{ij}$ and $\hat{\mathbf{y}}_{ij}$ and next apply a polynomial model to fit the HRB edges from the samples.

Without any loss of generality, the following polynomial regression model

$$f(x) = c_0 + c_1 x^1 + c_2 x^2 + \cdots + c_k x^k \tag{1}$$

is applied. In our case, we aim to measure the diameter of a cylindrical HRB. Therefore, a first order polynomial regression model is sufficient. By assigning $c_1 \triangleq a_{ij}$ and $c_0 \triangleq b_{ij}$, we have a linear model

$$f_{ij}(x) = a_{ij}x + b_{ij}. \tag{2}$$

After the HRB edges are fitted, we use (2) to generate a new set of points to represent the corresponding HRB edges. In our case, we set

$$\mathbf{x}_{ij} = [(i-1) * H + 1, \cdots, i * H], \tag{3}$$

and $\mathbf{y}_{ij}$ is then produced by

$$\mathbf{y}_{ij} = a_{ij}\mathbf{x}_{ij} + b_{ij}. \tag{4}$$

The black line segments in Figures 3 (c) and (d) show the results of Algorithm 2. The results shown in these figures are obtained after $T = 10$ times sampling from each CBOI. We can see that, if the CBOIs are not severely corrupted, the line segments from the sliding window random regression algorithm define well the HRB edges. However, when CBOIs are corrupted, the line segments from the sliding window random regression algorithm no longer represent the HRB edges accurately. Here, we first provide the transformation from the image plane to the physical plane. The treatment of the measurement uncertainty will be given in the next section.

In our case, two HRB edges are expected within the sliding window $I_{H\times W}$. Therefore, we set up all n_i to be equal to $n = 2$. The $\mathbf{x}_{ij}$ and $\mathbf{y}_{ij}$ coordinates from the image plane are converted to coordinates in the physical plane through the transformation

$$\begin{bmatrix} x_{ij}^w \\ y_{ij}^w \\ z_{ij}^w \\ 1 \end{bmatrix} = \begin{bmatrix} \mathbf{R} & \mathbf{T} \\ \mathbf{0} & \mathbf{1} \end{bmatrix} \mathbf{K} \begin{bmatrix} x_{hj}^I \\ y_{hj}^I \\ 1 \end{bmatrix}, \tag{5}$$

where $\mathbf{R}$ and $\mathbf{T}$ are respectively the rotation and translation matrices, and $\mathbf{K}$ is the intrinsic matrix of the camera parameters. These matrices are obtained via the calibration process. The coordinates $x_{ij}^I \in \mathbf{x}_{ij}$ and $y_{ij}^I \in \mathbf{y}_{ij}$ are from the image plane and $[x_{ij}^w, y_{ij}^w, z_{ij}^w, 1]^T$ is the vector of corresponding coordinates in the physical plane. Given the vectors $I_{i1} = [x_{i1}^I, y_{i1}^I]^T$ and $I_{i2} = [x_{i2}^I, y_{i2}^I]^T$ on two HRB edges with $x_{i1}^I = x_{i2}^I$, the diameter l of the HRB is then calculated through

$$l = \|P_1 - P_2\|_2, \tag{6}$$

with $P_1 = [x_{i1}^w, y_{i1}^w]^T$ and $P_2 = [x_{i2}^w, y_{i2}^w]^T$, which are physical plane correspondences to I_{i1} and I_{i2}. Here $\|.\|_2$ denotes the Euclidean norm.

III. Weighted Variance for Uncertainty Quantification

Similarly to the measurement accuracy, the level of trust in the measurements is also essential to this task as it supports downstream decision-making. In this paper, we quantify the measurement uncertainties on the final results with the weighted variance as part of the Algorithm 3. In our case, the trust level reflects how severely the measurements are affected by corrupted CBOIs along with other noises. Figures 4(a) and (b) show well determined boundaries of interest, while Figures 4(c) and (d) show boundaries of interest with corrupted CBOIs. When the measurements are from corrupted CBOIs, the variance value will go high.

Given the i-th sliding window, there are n_i CBOIs in it, and each corresponds to a B_j with $j \in \{1, \cdots, n_i\}$. For each B_j, we sample T times, each time with S point pairs from $\hat{\mathbf{x}}_{ij}$ and $\hat{\mathbf{y}}_{ij}$. From each point pair, we use (5) and (6) to calculate S diameters, which are further averaged to find the representative diameter value l_{it}, with $t = 1, \cdots, T$. Then the measurement and variance in the current sliding window are calculated respectively from

$$l_i = \sum_{t=1}^{T} l_{it}/T, \ \sigma_i = \sqrt{\sum_{i=1}^{T} (l_{it} - l_i)^2/T}. \tag{7}$$

With the sampling strategy, impacts of the corrupted CBOIs on the measurements are mitigated, especially when the area of a CBOI is small. However, when the area of a corrupted CBOI is big, it becomes difficult to use the fitted line segments to represent the HRB edges. The reason lies in that compared with samples constrained in a smaller CBOI, samples from

Algorithm 3 Uncertainty Quantification

Input: $\hat{\mathbf{x}}_{ij}$ and $\hat{\mathbf{y}}_{ij}$ after clustering, a binary sliding window $I_{H\times W}$, and sampling times T.

Output: diameter l_i and weighted variance Σ_i

1: **for** $i = 1, \cdots, m$ **do**
2: CBOI areas in current window, $A_{i1}, \cdots, A_{in_i}$, with average $A_i = \sum_{j=1}^{n_i} A_{ij}/n_i$, and similarity ratio $\mathcal{R}_i = A_i/C$.
3: Calculate weight $\mathcal{L}_i$ from (9).
4: Weighted variance calculation from (10).
5: **end for**

a bigger CBOI are more dispersed. Hence, we consider this CBOI area for quantifying the measurement uncertainty.

In this paper, we have taken the CBOI areas into consideration by using CBOI areas as weights, and each σ_i from (7) is then adjusted by the weight. To achieve that, for the i-th sliding window, we first calculate the area of each CBOI within it and get the respective areas $A_{i1}, \cdots, A_{in_i}$. A similarity ratio $\mathcal{R}_i$ is next calculated via

$$\mathcal{R}_i = \Big(\sum_{j=1}^{n_i} A_{ij}/n_i\Big)/C, \tag{8}$$

where C is the average area of uncorrupted CBOIs. We use it to normalise the similarity ratio. Figure 3 (c) shows an uncorrupted CBOI and C is the area of the region marked in dark blue. The values of the similarity ratio $\mathcal{R}_i$ could fall into the following three cases: *1)* $\mathcal{R}_i < 1$, *2)* $\mathcal{R}_i = 1$, and *3)* $\mathcal{R}_i > 1$. We would prefer the first two cases because it means $A_{i1}, \cdots, A_{in_i}$ are on average smaller or equal to C. This indicates that samples from the corresponding CBOIs are constrained in small areas, and line segments fitted from these samples are more likely to align with the HRB edges. On the contrary, when the third case happens, we would know that the samples are from CBOIs with areas greater than C, which will increase the chance that fitted line segments from these samples are unaligned with HRB edges. To convey the information, we, therefore, define the variance weight as

$$\mathcal{L}_i = \mathcal{R}_i^2 * \exp(\mathcal{R}_i - 1),\ i = 1, \cdots, m. \tag{9}$$

We use $\mathcal{R}_i^2$ to indicate that the weight is proportional to the CBOI area. It is obvious that $\mathcal{R}_i$ values greater than 1 would lead to greater $\mathcal{L}_i$, when compared with $\mathcal{R}_i$ values equal to or are smaller than 1.

We now give the trust level in the measurements as

$$\Sigma_i = \mathcal{L}_i * \sigma_i,\ i = 1, \cdots, m. \tag{10}$$

Note that a big value of Σ_i means a reduced trust in the measurement, compared with a measurement with a small Σ_i value. The bigger the Σ_i value is, the more scattered the measurement is, in a wide area.

IV. Performance Validation and Evaluation

To demonstrate the effectiveness of the framework, we processed video frames captured by a GoPro® Hero 7 Black camera with Matlab 2018a programs. The PC configuration includes an Intel(R) Core(TM) i7-7800X CPU and 16.0GB RAM. The 2.7K camera mode is used and the shutter speed is set up to $1/480$ s, to restrain the distortion and overexposure. The camera is calibrated on the scene with a checkerboard of 8×5 squares of size 50×50 mm. Although the whole HRB is visible in the images, we only focus on the region where the checkerboard was placed to exclude errors caused by calibration parameters. The ground-truth diameter of the HRB is 265.5 mm. The parameters α and β are set to 0.95 and 240, respectively. Here the height H is equal to 5 pixels and the width W of the image is equal to 2704 pixels. Table I shows the average computational costs of each algorithm. The computational time is suitable for real time applications since the HRBs move slowly (even stop for sawing the ends) on the conveyor.

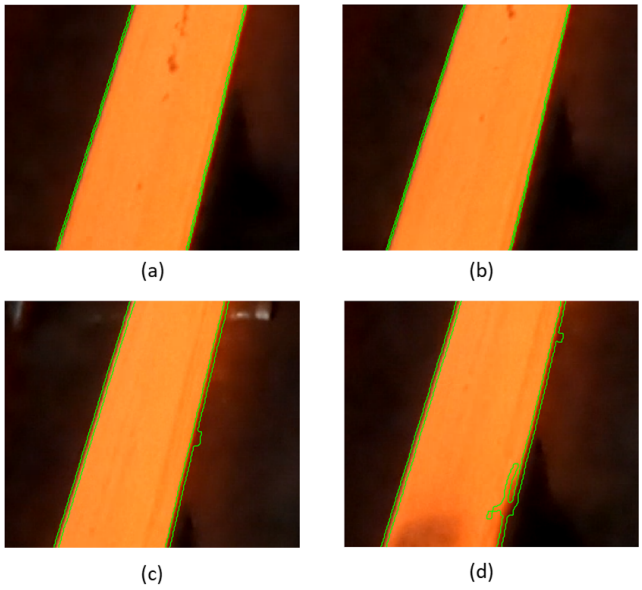

Fig. 4. Boundaries of interest from four randomly selected images

TABLE I
Efficiency evaluation of the algorithms

	Algorithm 1	Algorithm 2	Algorithm 3
Time(ms)	407	38	52

Figure 5 shows results from the proposed framework. For a compact representation of the results, we have aggregated the HRB diameter ground-truth (265.5 mm) and the tolerance zone ($[265.5 - 3.0$ $mm, 265.5 + 3.0$ $mm]$), the measurements from our framework, and the weighted variance for uncertainty quantification into a single figure. In each sub-figure, the x-axis indicates the number of sliding windows. The left y-axis shows the ground-truth, measurements, and the tolerance zone. The right y-axis shows only the one Σ interval, to show the trust level in the diameter measurement. Compared with the narrower Σ intervals, a wider one Σ interval (or even a peak

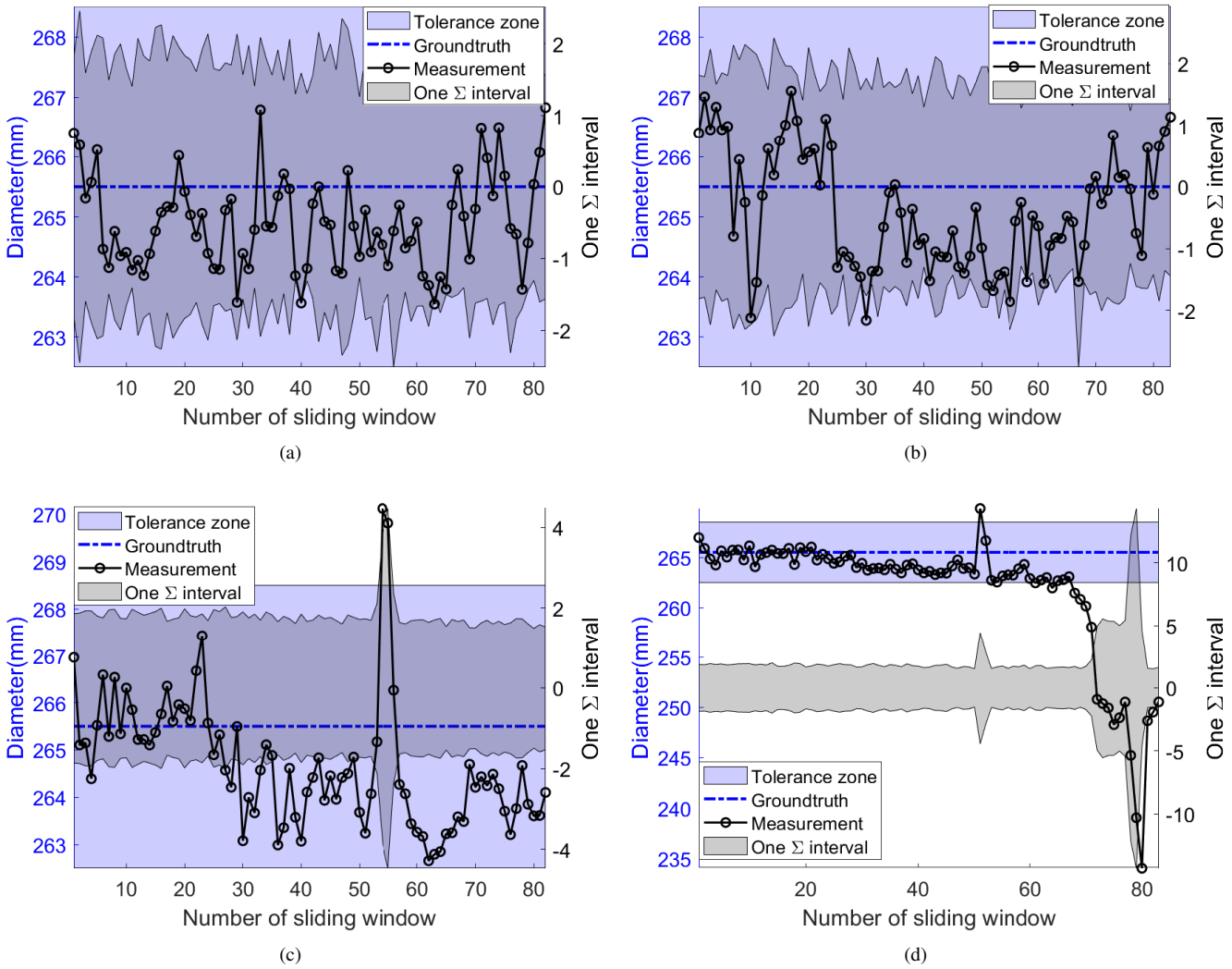

Fig. 5. Diameter measurements and trust level from four randomly-selected frames: (a) and (b), measurements with high trust level, (c) measurements correspond to one corrupted CBOI, (d) measurements correspond to two corrupted CBOIs.

interval) means a reduced level of trust in the measurement, as it means to us that the measurement scatters in a big area.

The measurement is not necessarily enclosed by the one Σ interval due to different scales of the two y-axes. However, the trends of the one Σ interval and the corresponding measurement should be kept consistent. Especially, the one Σ interval should convey the information when the measurement goes over the tolerance zone.

For instance, we can see in Figures 5(a) and 5(b) that, the measurements fluctuate around the ground-truth and the one Σ intervals change in accordance. There are no dramatic changes of the measurements or the one Σ intervals observed in these two figures. All the measurements are bounded by the tolerance zone. This indicates that these measurements are trust-able. In fact, Figures 5(a) and 5(b) show typical results from images that are similar to Figures 4(a) and 4(b), where the CBOIs are not corrupted.

In comparison, when CBOIs are corrupted as shown in Figures 4(c) and 4(d), we can observe drastic changes of the measurements and the one Σ intervals. Typical results are shown in Figures 5(c) and 5(d). There are one prominent measurement peak in Figure 5(c) and two in Figure 5(d). We can see measurements corresponding to the peaks go over the tolerance zone, and thus should not be trusted. With our proposed uncertainty quantification algorithm, this information is encoded in the corresponding one Σ interval. As can be seen from Figures 5(c) and 5(d), wide one Σ intervals emerge in accordance with the measurement peaks. Therefore, the one Σ interval would provide us with a trust level in the measurements.

With the proposed framework, when the one Σ interval changes drastically, we would discard (not trust-able) the corresponding measurements. While we have shown measurements within sliding windows in Figure 5, we now give measurements from a whole frame by integrating all the trust-able measurements from the sliding windows. For frame-wise

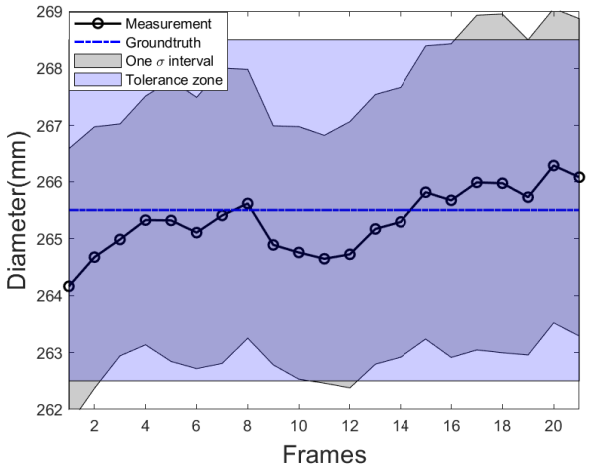

Fig. 6. Diameter measurements from frames

measurements, we use the following relations to calculate the measurement and variance.

$$\bar{l}_i = \sum_{i=1}^{m_f} l_i/m_f,\ \sigma = \sqrt{\sum_{i=1}^{m_f} \left(l_i - \bar{l}_i\right)^2/m_f}, \qquad (11)$$

where m_f is the number of the processed frames.

The frame-wise measurements are shown in Figure 6. Note that the x-axis now indicates the frame numbers. Since measurements from corrupted CBOIs are discarded, we now use (11) to represent the one σ interval. Be aware that the weighted variance Σ is used to quantify measurement uncertainty, while σ here is just a normal variance describing how spread out the frame-wise measurements are. We can see that the difference between each measurement and ground-truth pair is within $[-2.5\ mm, 2.5\ mm]$, which is in line with the rolling standards $[-3.0\ mm, 3.0\ mm]$.

V. Conclusion

In this paper, a computer vision framework is proposed to measure the diameter of hot rolled steel bars. We detect and constrain the edges of HRBs within a boundary of interest accounting for uncertainties. The sliding window random regression algorithm is then applied to sample from CBOIs and fit the HRB edges in the image plane, which are further transformed to the physical plane for diameter calculation. To reflect the impacts of environmental noise and corrupted CBOIs on the measurements, we present the weighted variance algorithm and this provides trust levels in the measurements.

With the proposed framework, we have successfully segmented HRBs in images and provide the diameter estimates with acceptable accuracy. The weighted variance enables uncertainty quantification on the measurements and ultimately provides a trust level to discard outlier measurements, resulting in accurate diameter measurements.

Our future work will continue in three directions: *1*) Deploying the developed framework in the factory to help our industrial partner to monitor the production process in real time; *2*) Applying three dimensional reconstruction to obtain dimensional measurements of steel sections of different shapes; *3*) Fusion of thermal and optical images for autonomous size measurement of the HRBs.

Acknowledgements. We are grateful to our sponsors through the Knowledge Exchange grant (Internet of Things for Overcome Barriers in the Steel Rolling Measurement Technology) with the Liberty Speciality Steels, the EPSRC IAA grant R/164995-11-1. We also thank NSFC(61703387). We are grateful to EPSRC for funding this work through EP/T013265/1 project NSF-EPSRC:ShiRAS. Towards Safe and Reliable Autonomy in Sensor Driven Systems. This work was also supported by the National Science Foundation under Grant NSF ECCS 1903466.

References

[1] J. Zhu, M. Li, Y. Jiang, T. Xie, F. Li, C. Jiang, R. Liu, and Z. Meng, "Research on online 3d laser scanner dimensional measurement system for heavy high-temperature forgings," in *Proceedings of the AOPC 2017: 3D Measurement Technology for Intelligent Manufacturing*, vol. 10458, 2017, pp. 104 581Q–1–104 581Q–9.

[2] B. Wang, W. Liu, Z. Jia, X. Lu, and Y. Sun, "Dimensional measurement of hot, large forgings with stereo vision structured light system," *Journal of Engineering Manufacture*, vol. 225, no. 6, pp. 901–908, 2011.

[3] W. Liu, Z. Jia, F. Wang, X. Ma, W. Wang, X. Jia, and D. Song, "An improved online dimensional measurement method of large hot cylindrical forging," *Measurement*, vol. 45, no. 8, pp. 2041–2051, 2012.

[4] J. Yang, W. Liu, R. Zhang, Z. Jia, F. Wang, and S. Li, "A method for measuring the thermal geometric parameters of large hot rectangular forgings based on projection feature lines," *Machine Vision and Applications*, vol. 29, no. 3, pp. 467–476, 2018.

[5] A. Zatočilová, D. Paloušek, and J. Brandejs, "Image-based measurement of the dimensions and of the axis straightness of hot forgings," *Measurement*, vol. 94, pp. 254–264, 2016.

[6] B. Wu, F. Zhang, and T. Xue, "Monocular-vision-based method for online measurement of pose parameters of weld stud," *Measurement*, vol. 61, pp. 263–269, 2015.

[7] P. Dollár and C. L. Zitnick, "Fast edge detection using structured forests," *IEEE Transactions on Pattern Analysis and Machine Intelligence*, vol. 37, no. 8, pp. 1558–1570, 2014.

[8] M. A. Oskoei and H. Hu, "A survey on edge detection methods," *University of Essex, UK*, vol. 33, 2010.

[9] X. S. Poma, E. Riba, and A. Sappa, "Dense extreme inception network: Towards a robust cnn model for edge detection," in *The IEEE Winter Conference on Applications of Computer Vision*, 2020, pp. 1923–1932.

[10] P. Wang, Y. Lin, R. Muroiwa, S. Pike, and L. Mihaylova, "Computer vision methods for automating high temperature steel section sizing in thermal images," in *2019 Sensor Data Fusion: Trends, Solutions, Applications (SDF)*. IEEE, 2019, pp. 1–6.

[11] N. Otsu, "A threshold selection method from gray-level histograms," *IEEE Transactions on Systems, Man and Cybernetics*, vol. 9, no. 1, pp. 62–66, 1979.

[12] P. Soille, *Morphological image analysis: principles and applications*. Springer Science & Business Media, 2013.

[13] T. H. Mandeel, M. I. Ahmad, M. N. M. Isa, S. A. Anwar, and R. Ngadiran, "Palmprint region of interest cropping based on moore-neighbor tracing algorithm," *Sensing and Imaging*, vol. 19, no. 1, p. 15, 2018.

[14] K. Krishna and M. N. Murty, "Genetic k-means algorithm," *IEEE Transactions on Systems, Man, and Cybernetics, Part B (Cybernetics)*, vol. 29, no. 3, pp. 433–439, 1999.